THE ASTROPHYSICAL JOURNAL, 548:L111–L114, 2001 February 20

A LIMIT ON THE POLARIZED ANISOTROPY OF THE COSMIC MICROWAVE BACKGROUND AT SUBDEGREE ANGULAR SCALES

M. M. HEDMAN, D. BARKATS, J. O. GUNDERSEN,[1] S. T. STAGGS,[2] AND B. WINSTEIN[3]
Joseph Henry Laboratories and Physics Department, Princeton University, Princeton, NJ 08544
Received 2000 October 30; accepted 2000 December 18; published 2001 February 19

ABSTRACT

A ground-based polarimeter, PIQUE, operating at 90 GHz has set a new limit on the magnitude of any polarized anisotropy in the cosmic microwave background. The combination of the scan strategy and full width half-maximum beam of 0.°24 gives broad window functions with $\langle l_E \rangle = 211^{+294}_{-146}$ and $\langle l_B \rangle = 212^{+229}_{-135}$ for the *E*- and *B*-mode window functions, respectively. A joint likelihood analysis yields simultaneous 95% confidence level flat band power limits of 14 and 13 μK on the amplitudes of the *E*- and *B*-mode angular power spectra, respectively. Assuming no *B*-modes, a 95% confidence limit of 10 μK is placed on the amplitude of the *E*-mode angular power spectrum alone.

Subject headings: cosmic microwave background — cosmology: observations — polarization

1. INTRODUCTION

Observations of the temperature anisotropies of the cosmic microwave background (CMB) already constrain cosmological models (e.g., Tegmark & Zaldarriaga 2000). In addition, a linearly polarized component of the CMB arises from any quadrupolar variation in the photons scattered from electrons at the last scattering surface (Rees 1968; Hu & White 1997). Polarization data will complement other CMB data (e.g., Kosowsky 1999). Current cosmological models predict that polarization anisotropies are 10–20 times smaller than temperature anisotropies. To date, only upper limits on the CMB polarization exist, summarized in Staggs, Gundersen, & Church (1999) and Subrahmanyan et al. (2000). The polarization fluctuations may be decomposed into gradient and curl parts (Kamionkowski, Kosowsky, & Stebbins 1997), here designated *E*- and *B*-modes (Zaldarriaga & Seljak 1997). The complete formalism for analyzing polarization data developed by these authors, and extended in Zaldarriaga (1998, hereafter Z98), is applied to data here for the first time.

2. INSTRUMENT

The Princeton IQU Experiment[4] (PIQUE) comprises a single 90 GHz correlation polarimeter underilluminating a 1.2 m off-axis parabola (Wollack et al. 1997). The beam on the sky is 0.°235, and the instrument observes a single Stokes parameter in a ring of radius 1° around the north celestial pole. The receiver is a heterodyne analog correlation polarimeter using W-band (84–100 GHz) high electron-mobility transistor (HEMT) amplifiers. A mechanical refrigerator cools the corrugated feed horn, the orthomode transducer (OMT), and the HEMT amplifiers to $\lesssim$40 K. The telescope is fixed in elevation but rotates in azimuth. Two large nested ground shields surround the instrument; the inner shield rotates with the telescope.

The correlation polarimeter (Krauss 1986) directly measures the polarized electric field, rather than detecting and then differencing two large intensity signals. The two input signals come from an OMT oriented so one arm is parallel to the azimuthal scan direction. The polarimeter output is proportional to the linear polarization for axes rotated 45° with respect to the inputs. The local oscillator signal in one polarimeter arm is phase switched at 4 kHz, well above the 1 kHz 1/*f* knee of the amplifiers (Wollack & Pospieszalski 1998). The 2–18 GHz intermediate-frequency (IF) band is split into three frequency channels (S0, S1, S2). The total power in each of the IF arms is also detected, although with significantly less sensitivity since the phase switching does not apply. The polarimeter characteristics are given in Table 1.

3. OBSERVATIONS AND CALIBRATION

Between 2000 January 19 and 2000 April 2, PIQUE collected slightly over 800 hr of data from the roof of the physics building at Princeton, latitude 40.°345, east longitude −74.°647. Every 5 s, the telescope alternated between two azimuth positions, $\pm 0.°93$, at elevation 41.°04, measuring $\mp Q$ (as defined by the IAU) for two regions separated by 06^h in right ascension (R.A.) on the $\delta = 89°$ ring.

Since the polarimetry channels have a small (<23 dB) sensitivity to total power, PIQUE differences data taken in the east position from data taken in the west position 5 s later. Residual offsets in these "chopped" data, listed in Table 1, are small and stable (1/*f* knee undetectable at 10 μHz in clear weather). The offsets have been traced to polarized emissive pickup from the fixed ground screen and are removed as described below. Since Q is measured in the west and $-Q$ is measured in the east, the chopped data comprise sums of Stokes parameter Q.

Constant elevation scans of Jupiter are used to determine pointing accuracy, map the beams, and calibrate the total power channels. The absolute errors in elevation and azimuth are 0.°01 and 0.°02, respectively. The beam FWHMs are 0.°233(9) (cross-elevation) and 0.°240(14) (elevation), in agreement with calculations and near-field data. For the purpose of the likelihood analysis, the beam dispersions are taken as $\sigma = \theta^{\rm FWHM}_{\rm avg}/(8 \ln 2)^{1/2} = 0.°1$. Uncertainty in the brightness temperature of Jupiter contributes to a 10% error in the calibration of the total power channels (which are used only to correct for the slowly varying atmospheric opacity during the CMB polarization observations).

The polarimetry channels are calibrated by observations of the polarized emission (and reflection) from a large ambient-

[1] Robert H. Dicke Fellow.
[2] Alfred P. Sloan Fellow.
[3] Department of Physics and the Enrico Fermi Institute, University of Chicago, Chicago, IL 60637.
[4] Three of the four Stokes parameters are *I*, *Q*, and *U*. PIQUE measured *I* and *Q* in 2000 and will add *U* in 2001.

TABLE 1

PIQUE 2000 POLARIMETER CHARACTERISTICS

Channel	$\nu_c(\Delta\nu)$[a] (GHz)	S[b] (mK $s^{1/2}$)	T_{off}[c] (μK)	$\bar{\sigma}$[d] (μK)
S0	87.0(4.0)	2.3	−20(10)	25
S1	91.5(4.8)	2.3	330(30)	26
S2	96.2(2.3)	3.4	600(30)	41

NOTE—All temperatures are in thermodynamic units.

[a] Effective center frequencies and bandwidths, including gain slope and phase match degradations.

[b] Raw sensitivity measured on a clear day with $T_{atm} \approx 45$ K, uncorrected for atmospheric opacity. The differencing strategy degrades the sensitivity by a factor of 2.

[c] Average chopped offset where the error gives the standard deviation of the mean of the 11 offsets calculated during the season; see text. The typical statistical error in calculation of a single one of the 11 offsets is 20 μK.

[d] The average error per bin for the final data binned into 24 0.°26 wide R.A. bins. Note that the analysis uses data in 144 bins.

temperature aluminum flat. Nutating the flat about a vertical axis results in a peak-to-peak polarized signal of about 30 mK. These measurements are consistent with polarized cold load tests. The final calibration error is 10%, dominated by uncertainty in the surface resistivity (4.0 $\mu\Omega$ cm) of the nutating flat.

4. DATA REDUCTION

Of the 807 hr of data, 200 hr were spent slewing the telescope, 123 hr were corrupted by various electromechanical failures, and 52 hr were isolated segments less than 8 hr in duration which are not used. High levels of atmospheric noise contaminated 102 of the remaining 432 hr, as determined by the large positive tails in the distributions of the polarization channels' correlation coefficients. In order to avoid biasing the data set, the primary atmosphere cut employs the quadrature chop data. A quadrature chop has the raw data from each azimuthal position (east and west) split in two to obtain $(E_1 + W_1 - E_2 - W_2)/2$, which contains no polarization signal. This cut removes 78 hr by requiring the absolute values of all three correlation coefficients for 10 minute sections of the quadrature data to lie below a threshold, $\eta_q = 0.32$. Varying η_q by $\pm 5\%$ does not affect the final results statistically. The secondary atmosphere cut removes occasional unexplained transient polarized signals by culling extreme values (>4 σ from the mean) of the polarization channels' correlation coefficients. This cut removes an additional 24 hr of data.

The final data cut makes use of the 6 hr null test. The 6 hr null test takes advantage of the fact that certain linear combinations of data separated by 06^h in R.A. should have zero signal: $d_t - d_{t+6} + d_{t+12} - d_{t+18} = 0$, where t is measured in hours. Those days that fail this null test $[p(\chi^2|\nu) < 0.05]$ are removed. This final cut removes an additional 82 hr of data, leaving 248 hr of CMB data for the final analysis. Note that while this cut only slightly increases the final limits, it significantly improves the H1−H2 null test described below.

The remaining time series is binned into ≈2100 10^m wide bins. The means, standard deviations, and interchannel correlations are calculated for each bin. The attenuation due to atmospheric opacity for each bin is estimated from a total power channel and the appropriate (≈15%) correction is applied. The data are divided into 11 periods separated from one another by stretches of weather severe enough to require covering the instrument. The periods have varying lengths t_i, where 16 hr $< t_i <$ 110 hr. An offset for each channel is calculated and removed from each period. Other divisions of data, in which as few as two or as many as 24 offsets are removed, do not change the limit by more than 1 μK. The weighted means, standard deviations, and covariances are calculated for 144 10^m R.A. bins. These data are rebinned for presentation in Figure 1.

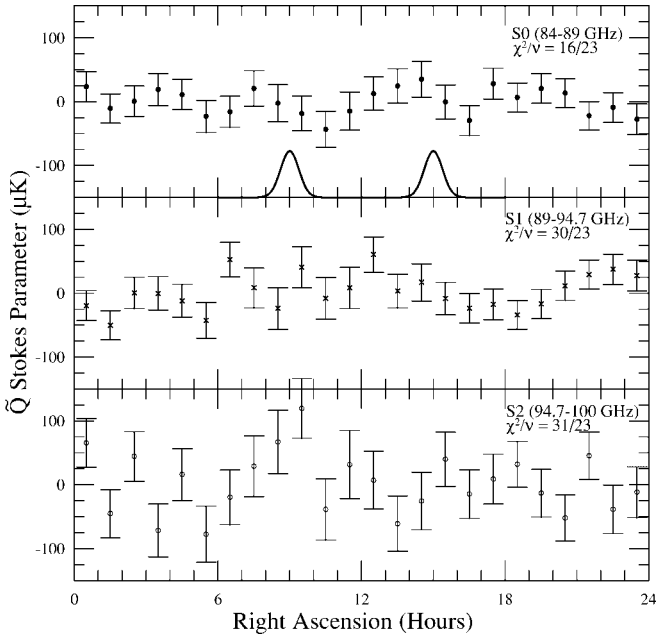

FIG. 1.—Binned data in thermodynamic units for each frequency channel, vs. R.A. For this plot, 24 approximately beam-sized bins are shown, although the analysis uses 144 bins. The theoretical point source response to a 250 mJy polarized source is indicated in the top panel.

Table 2 presents the results of a series of null tests. The null data sets include the quadrature data, data differenced between the first and second halves of the observing run (H1−H2), data differences between signal channels, and the 6 hr null data. The χ^2 distribution of the null tests is consistent with noise. Similarly, no contamination is found when the data are binned in Sun-centered or Moon-centered coordinates.

5. DATA ANALYSIS

The Bayesian method with uniform prior is used to establish limits on the amplitude of the polarization anisotropy and to verify null tests of the data. The data vector d has $3N$ entries, where $N = 144$. The data covariance matrix C_D consists of nine $N \times N$ diagonal submatrices, since correlations between 10^m bins are small enough to neglect (≪1% of the variances). Six of the submatrices account for interchannel correlations due to HEMT-induced correlated gain fluctuations and correlations from atmospheric fluctuations weakly coupled into the

TABLE 2

RESULTS OF χ^2 CONSISTENCY TESTS

Data[a]	ν[b]	S0[c]	S1[c]	S2[c]
CMB	143	0.73	0.11	0.88
Quadrature	143	0.95	0.06	0.57
H1−H2	143	0.28	0.24	0.37
6 hr null	36	0.19	0.32	0.97
		S0−S1	S0−S2	S1−S2
Interchannel	143	0.32	0.66	0.61

[a] The data sets are described in the text.

[b] The number of degrees of freedom for each data set.

[c] The probability of exceeding the χ^2 for a given frequency channel.

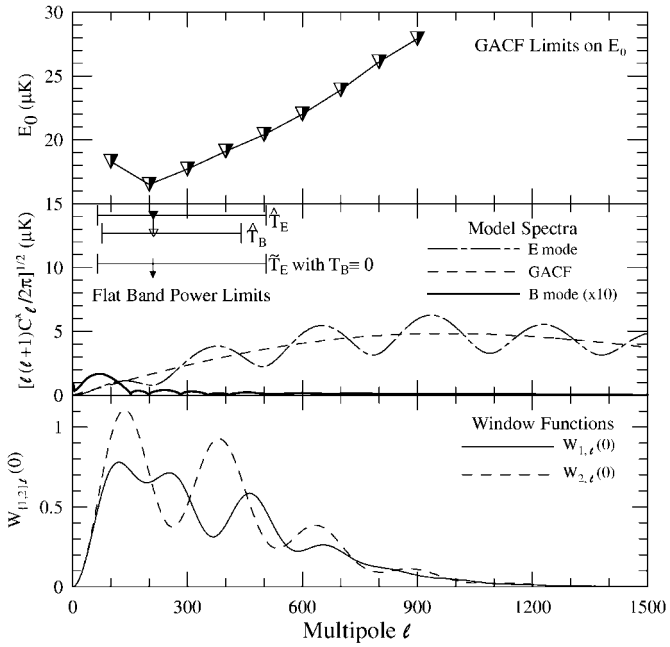

FIG. 2.—Zero-lag window functions for *E*- and *B*-modes (*solid and dashed lines*) are plotted in the lower panel. The middle panel shows the limits on T_E and T_B described in the text, plotted over *E*-mode predictions (*dash-dotted line*) from the $\Omega_{tot} = 1$ model of Jaffe et al. (2001) and *B*-mode predictions (*solid line*, assuming $T/S = 1$). The dashed curve is a GACF with $E_0 = 5.6$ μK and $l_c = 687$. To illustrate PIQUE's ability to limit the fluctuations where they are thought to be sizeable, the top panel shows the 95% confidence limits on the amplitude of the GACF, E_0, where the abscissa is $l_p = \sqrt{2}l_c$.

polarimeter channels. The average correlation coefficients between S0−S1, S0−S2, and S1−S2 are 0.02, 0.08, and −0.01, respectively. The theory covariance matrix C_T may be expressed in terms of the *E*- and *B*-mode angular power spectra C_l^E and C_l^B by

$$C_T^{ij} = \langle \tilde{Q}(\hat{n}_i)\tilde{Q}(\hat{n}_j)\rangle = \frac{1}{4\pi}\sum_{l=2}^{\infty}(2l+1)[C_l^E W_{1,l}(\phi_{ij}) + C_l^B W_{2,l}(\phi_{ij})], \quad (1)$$

where $\hat{n}_{i,j}$ are position vectors, $\phi_{ij} = \cos^{-1}(\hat{n}_i \cdot \hat{n}_j)$ is the lag, and $W_{1,l}$ and $W_{2,l}$ are associated window functions. The Q indicates that PIQUE measures sums of Q-values. Z98 presents an elegant way to describe the window functions for a ring observation strategy, here modified to include the PIQUE differencing:

$$W_{\{1,2\},l}(\phi_{ij}) = 2\sum_{m=1}^{l} F^2_{\{1,2\},lm}(\theta)B^2_{lm}\cos(m\phi_{ij}), \quad (2)$$

where the factor of 2 in front accounts for the negative *m*-values, and the $m = 0$ term is excluded from the window functions because offsets are removed from the data. The $F_{\{1,2\},lm}$ are given in Z98 in terms of associated Legendre polynomials, $\theta = 1°$ is the radius of the ring, and

$$B_{lm} = 2\cos(m\alpha/2)\frac{\sin(m\Delta\phi/2)}{(m\Delta\phi/2)}e^{-l(l+1)\sigma^2/2}, \quad (3)$$

where $\alpha = \pi/2$ is the chop amplitude and $\Delta\phi = \pi/72$ is the bin size. The window functions are depicted in Figure 2. The

TABLE 3
95% CONFIDENCE LIMITS

Data[a]	$\tilde{T}_E$[b] (μK)	$\hat{T}_E$[c] (μK)	$\hat{T}_B$[c] (μK)	E_0[d] (μK)
CMB	10	14	13	17
Quad	11	14	13	18
(H1−H2)/2	12	17	15	18

[a] The data sets are described in the text.
[b] The limit $\tilde{T}_E$ is found assuming $T_B \equiv 0$.
[c] The limits $\hat{T}_E$ and $\hat{T}_B$ are determined simultaneously by finding the contour of constant likelihood enclosing 95% of the volume.
[d] The limit on the amplitude of the GACF, E_0, at $l_p = 200$.

likelihood is $\mathcal{L} \propto \exp(-d^T M^{-1} d/2)/(|M|)^{1/2}$, where $M = C_T + C_D$.

The likelihood analysis proceeds by first considering flat angular spectra, such that $l(l+1)C_l^X/2\pi = T_X^2$, where $X = E, B$. Since the amplitude of C_l^B is predicted to be much smaller than that of C_l^E (see Fig. 2), Table 3 presents the limit on T_E under the assumption $T_B \equiv 0$. Figure 3 shows $\mathcal{L}(T_E, 0)$ for the CMB data and two null data sets. The limit $\tilde{T}_E$ is found by integrating $\mathcal{L}(T_E, 0)$; the result is ≈30% higher if $\mathcal{L}(T_E^2, 0)$ is integrated. Next, joint upper limits $(\hat{T}_E, \hat{T}_B)$ are determined by finding the constant contour of $\mathcal{L}(T_E, T_B)$ enclosing 95% of the volume of $\mathcal{L}$. Finally, a Gaussian autocorrelation function (GACF) analysis is performed. The motivation to revive the GACF is that it better describes the gross features of the predicted *E*-mode spectrum than the flat model; see Figure 2. For the GACF with characteristic scale l_c, the power spectra are given by $l(l+1) \times C_l^X/2\pi = X_0^2 u^2 \exp(-u^2/2)$, where $X_0 = E_0, B_0$, $u \approx l/l_c$ (Bond 1995), and $l_p = \sqrt{2}l_c$ is the peak of the GACF. Only the case $B_0 \equiv 0$ is considered. The likelihood $\mathcal{L}(E_0, 0)$ is integrated to place 95% confidence level upper limits on E_0 for several values of l_p as shown in Figure 2. Table 3 summarizes the limits obtained for the CMB data and two null tests. Performing the likelihood analysis on 50 simulated data sets with the same sensitivity shows that the 95% confidence level limits for the null tests and the CMB data are within 1 standard deviation of one another. The limits in Table 3 do not include calibration errors (10%). Note that for PIQUE's broad window functions, the 7% beam errors only add 2% errors in quadrature with the calibration errors. Finally, we fit $\mathcal{L}(T_E, 0)$ to an offset lognormal distribution as advocated by Bond, Jaffe, & Knox (2000), finding a central value of $T_E^2 = -3$ μK^2, a variance of (14 μK^2)^2, and a noise-related offset of 16 μK^2.

6. DISCUSSION

The formalism of Z98 enables us to place limits on both the *E*- and *B*-mode angular power spectra, allowing direct comparison of these results with theoretical expectations. Due to PIQUE's broad reach in *l*-space, these results limit the size of the predicted acoustic peaks in the polarization, rather than the damped tails at high and low *l*. PIQUE's limits on T_E and T_B

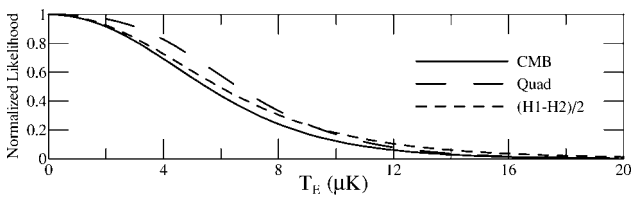

FIG. 3.—Normalized likelihoods for the cases when $T_B \equiv 0$

are higher than expected from, e.g., the $\Omega_{\rm tot} = 1$ model of Jaffe et al. (2001). The limits are also higher than expected foreground levels. Polarized dust emission anisotropy, extrapolated from the IRAS 100 μm map (Wheelock et al. 1994), should contribute $\lesssim 0.5$ μK, while polarized synchrotron, extrapolated from Brouw & Spoelstra (1976) or from Haslam et al. (1982), should be less than 0.4 μK. Spinning dust emission is even smaller (Draine & Lazarian 1999).

Since this paper represents the first effort to put limits on T_E and T_B directly, it is outside the scope of this paper to quantitatively compare these results to published results from previous experiments. Direct comparison would require other authors to reanalyze their data for sensitivity to *E*- and *B*-modes rather than to *Q* and *U*. Qualitatively, we note that the limit $\tilde{T}_E < 10$ μK is smaller by more than a factor of 2 than the best limits previously published for $l < 3000$ (Torbet et al. 1999; Netterfield 1995). Furthermore, PIQUE has sensitivity to higher l than these two previous experiments, so this work represents a significant improvement in the constraints on the polarization of the CMB.

We are indebted to Matias Zaldarriaga for insights on analysis of polarization experiments. We acknowledge M. Z. and Uroš Seljak for use of CMBFAST. We thank Ken Ganga, Chris Herzog, Norman Jarosik, Lloyd Knox, Lyman Page, Paul Steinhardt, and David Wilkinson for many helpful discussions and assistance. Much of the hardware for this experiment was adapted from the Saskatoon experiments. We are grateful to Ted Griffiths and Laszlo Varga for help in mechanical design and construction. We also thank Marian Pospieszalski and the NRAO for supplying the HEMT amplifiers. Data (including the correlation matrix and likelihood functions) will be made public upon publication of this Letter.

This work was supported by a NIST precision measurement grant NANB8D0061 and by NSF grant PHY 96-00015. Additional support was provided by the Alfred P. Sloan Foundation and the Guggenheim Foundation through their Fellowships for S. T. S. and B. W., respectively.

REFERENCES

Bond, J. R. 1995, Astrophys. Lett. Commun., 32, 63
Bond, J. R., Jaffe, A. H., & Knox, L. 2000, ApJ, 533, 19
Brouw, W. N., & Spoelstra, T. A. T. 1976, A&AS, 26, 129
Draine, B. T., & Lazarian, A. 1999, in Microwave Foregrounds, ed. A. de Oliveira-Costa & M. Tegmark (San Francisco: ASP), 133
Haslam, C. G. T., Salter, C. J., Stoffel, H., & Wilson, W. E. 1982, A&AS, 47, 1
Hu, W., & White, M. 1997, NewA, 2, 323
Jaffe, A., et al. 2001, Phys. Rev. Lett, in press (astro-ph/0007333)
Kamionkowski, M., Kosowsky, A., & Stebbins, A. 1997, Phys. Rev. D, 55, 7368
Kosowsky, A. 1999, NewA, 43, 147
Krauss, J. D. 1986, Radio Astronomy (2d ed.; Powell: Cygnus-Quasar Books)
Netterfield, C. 1995, Ph.D. thesis, Princeton Univ.
Rees, M. J. 1968, ApJ, 153, L1
Staggs, S. T., Gundersen, J. O., & Church, S. E. 1999, in Microwave Foregrounds, ed. A. de Oliveira-Costa & M. Tegmark (San Francisco: ASP), 299
Subrahmanyan, R., Kesteven, M. J., Ekers, R. D., Sinclair, M., & Silk, J. 2000, MNRAS, 315, 808
Tegmark, M., & Zaldarriaga, M. 2000, Phys. Rev. Lett., 85, 2240
Torbet, E., et al. 1999, ApJ, 521, L79
Wheelock, S. L., et al. 1994, *IRAS* Sky Survey Atlas: Explanatory Supplement (Publ. 94-11; Pasadena: JPL)
Wollack, E. J., Devlin, M. J., Jarosik, N., Netterfield, C. B., Page, L., & Wilkinson, D. 1997, ApJ, 476, 440
Wollack, E. J., & Pospieszalski, M. W., 1998, Proc. 1998 IEEE MTT-S Int. Microwave Symp. Digest, 669
Zaldarriaga, M. 1998, ApJ, 503, 1 (Z98)
Zaldarriaga, M., & Seljak, U. 1997, Phys. Rev. D, 55, 1830